Title
Optimization of in-vacuo template-stripped Pt surfaces via UHV STM

Journal
Applied Physics A, 80(6)

ISSN
0947-8396

Authors
Ohlberg, D
Blackstock, JJ
Ragan, R
et al.

Publication Date
2005-03-01

DOI
10.1007/s00339-004-3161-5

Appl. Phys. A 80, 1327–1334 (2005)
DOI: 10.1007/s00339-004-3161-5

Applied Physics A
Materials Science & Processing

D. OHLBERG[1,✉]
J.J. BLACKSTOCK[1,2]
R. RAGAN[1]
S. KIM[1,3]
R. STANLEY WILLIAMS[1]

Optimization of in-vacuo template-stripped Pt surfaces via UHV STM

[1] Quantum Science Research Group, Hewlett Packard Laboratories, 1501 Page Mill Road, MS 1123, Palo Alto, CA 94304, USA
[2] Department of Physics, Avadh Bhatia Physics Laboratory, University of Alberta, Edmonton, AB, T6G 2J1, Canada
[3] Department of Chemistry, Korea Advanced Institute of Science and Technology, 373-1 Guseong-dong, Yuseong-gu, Daejeon, 305-701, Korea

Received: 15 September 2004/Accepted: 23 November 2004
Published online: 11 March 2005 •

ABSTRACT A recently demonstrated [1] in-vacuo template-stripping process is applied to the study of platinum films stripped from ultra-flat silicon-oxide surfaces. Template-stripped (TS) Pt surfaces, prepared with a range of post-deposition annealing times prior to being stripped from the templating surface in an ultra-high vacuum (UHV) environment, are examined by UHV scanning tunneling microscopy (STM). These studies reveal that without post-deposition annealing, TS Pt surfaces are largely made up of poorly-ordered, granular nanostructures undesirable for many applications. The post-deposition annealing treatments explored in the study result in the emergence and continuous growth of large smooth crystallites. Issues with crystallite orientation relative to the TS surface and artefacts arising as a result of the epoxy used in the template-stripping process are presented and discussed in relation to optimizing the template-stripping procedure for specific applications such as self-assembled monolayer (SAM) formation for molecular electronics.

PACS 68.37.Ef; 68.47.De; 68.55.Jk; 81.05.Bx; 81.15.Ef

1 Introduction

As we advance toward electronic devices on the nanoscale, a defect tolerant architecture in the form of a cross bar array has been proposed for logic and memory applications that allows for scaling of junctions down to the molecular level [2–5]. The individual devices (junctions) in this architecture consist of one or more organic molecules interposed between electrical leads. Current efforts at our laboratory are focusing on the fabrication of arrays of such devices in this cross point architecture. In this scheme, a parallel series of nanoscale metal wire electrodes is fabricated and then coated with a layer of organic material. After the organic deposition, a second series of parallel nanoscale metal wire electrodes is deposited over the organic layer and perpendicular to the first series of wires, resulting in a 2D array of cross bar devices. Using nanoimprint lithography to fabricate both sets of nanoscale wire electrodes, this scheme was recently implemented to demonstrate a 64 bit field programmable memory at a density of 6.4 Gbits/cm^2 [6].

✉ Fax: +1-650-857-8487, E-mail: doug_ohlberg@hp.com

At the junctions of these arrays, the organic layer consists of a single molecular monolayer, formed either as a Langmuir–Blodgett (LB) film or a self-assembled monolayer (SAM). Being only a monolayer, the thickness of this organic layer ranges from 1 to 4 nm (depending on the molecular compound comprising the monolayer). As a result, the roughness of the metal/organic interface has a substantial influence on device performance and yield. If the roughness of the metal surface prior to LB or SAM deposition is greater than the thickness of the organic monolayer, or if the surface is so disordered as to render the homogenous growth of SAM's impossible, then device yields decrease dramatically [7, 8]. Platinum (Pt) has been the material of choice for the metal leads in this architecture because of the ease of forming SAMs on its surface [9], its low intrinsic malleability, low surface diffusivity, and – most importantly – its compatibility with conventional CMOS processing. Unfortunately, Pt deposited by the usual methods of e-beam evaporation or sputter deposition is far too rough [10] to produce high yields of working molecular electronics devices.

A component of our research effort has therefore been focused on developing methods of fabricating smooth Pt surfaces that can easily be integrated into ULSI processing conditions. One approach to producing ultra-smooth metal surfaces has been the template-strip method, whereby metals with poor adhesion to silicon-oxide are deposited on prime polished silicon wafers with thin surface oxide layers that serve as ultra-smooth templates [7, 10, 11]. The metal-coated surface is then bonded to a substrate, usually by means of an epoxy to form a template-substrate sandwich. The final step of the process is the actual strip that occurs when the substrate is pulled from the template. The metal, now chemically bonded to the substrate wafer via the epoxy, easily detaches from the template upon which it was initially deposited, leaving a surface nearly as smooth as the initial template surface. Pt and Au films have previously been demonstrated using this technique with RMS surface roughness values of 0.1 nm and 0.2 nm, respectively, over (1 μm^2) as measured by AFM [10].

The template-strip method has proven popular among researchers studying self-assembly processes of organic molecules on noble metal surfaces, as the ultra smooth films are significantly cheaper and more convenient to handle than single crystal metal surfaces [12–15]. An added advantage of the process is that as long as the surface is bonded to the tem-

plate it can be kept in ambient for months, remaining as clean and uncontaminated as when it was initially deposited, until the moment it is stripped for further use [10]. This procedure has recently been enhanced to allow patterned ultra-flat surfaces to be produced and employed as the bottom electrodes of micron-sized cross-bar devices with SAM organic monolayers, resulting in a marked improvement in non-shorted device yields [7].

In order to understand the properties of molecular devices, it is necessary to have an understanding of the metal surfaces and the metal/organic interfaces at the atomic scale. Researchers employing the template-strip technique have a number of parameters – templating substrate morphology, metal deposition rate and conditions, substrate temperature during evaporation, and post-deposition (pre-stripping) annealing time in- or ex-vacuo – that can be systematically varied to optimize the structure of the final template-stripped (TS) surfaces for a particular application. However, very little is known about how adjusting these various parameters affects the structure of these surfaces at atomic length scales, because few of the previous studies on TS surfaces have carried out any characterization at this level. The main reason for this is that until recently, no process had been developed to prepare these surfaces in ultrahigh vacuum (UHV) conditions, where the majority of atomically sensitive surface analysis techniques are readily available.

We recently demonstrated a simple process to strip templated metal surfaces from their templates in UHV for subsequent examination, in-situ, by scanning tunneling microscopy (STM). The TS Pt surfaces were found to be predominantly (111) oriented under the preparation conditions employed in that study [1]. Expanding on our previous work, this study begins to explore a few of the variable fabrication parameters affecting the final atomic and nanoscale structure of the TS Pt surfaces. The focus herein is on the effect of post-deposition annealing on the TS Pt surfaces, and also includes a brief examination of the variation of the Pt evaporation rate on the un-annealed surfaces. We employ the same in-vacuo template-strip process developed previously [1] and continue with our use of UHV STM as our primary tool for analyzing the atomic and nanoscale structure of the freshly stripped Pt surfaces.

The collected data reveal how tightly coupled the structure of the final TS surface is to the post-deposition but pre-stripping annealing conditions, as well as how the appropriate choice of epoxy (or bonding method) to attach the TS film to the substrate is critical to eliminating epoxy related artifacts from influencing the TS surface structure. These results provide a basic understanding regarding several parameters affecting the TS surface fabrication process, providing a crucial starting point for the iterative optimization of the process parameters for specific applications.

2 Experimental section

The templating surfaces used in this study were pieces of prime polished 4″ Si(100) wafers with native oxide surfaces cleaved to dimensions compatible with the STM sample holders (typically 3–4 mm in width, 10 mm in length). These pieces were cleaned for fifteen minutes in piranha solution (a 1:3 volume ratio of 30% aqueous hydrogen peroxide solution and concentrated sulfuric acid) immediately prior to loading into the high vacuum metal deposition chamber. The piranha treatment not only removed organic contaminants from the templating surfaces, but also served to ensure that the templates had uniform oxide coverage. Pt films 120 nm thick were evaporated in high vacuum chambers in one of two deposition processes. The first was a slow process conducted in an electron beam (e-beam) evaporation system (base pressure $\leq 10^{-6}$ Torr) that began with an initial rate of 0.01 nm/s for the first 5 nm, ramped up to 0.05 nm/s for the next 10 nm, and increased again to a final rate of 0.1 nm/s for rest of the film. The second was a fast process done in a different e-beam evaporation system (base pressure $\leq 10^{-7}$ Torr) at a rate of 0.1 nm/s throughout the entire deposition. In both cases, the template pieces were at room temperature during the deposition process.

The substrates on which the TS Pt films were mounted were 3 mm by 12 mm pieces also cleaved from Si(100) wafers and pre-cleaned in piranha solution before being completely coated – front, back and sides – with a metal film consisting of an initial 15 nm layer of aluminium followed by 20 nm of Pt to ensure good electrical contacts between the substrate and the STM sample holder. Epo-Tek H 21D silver epoxy was used to bond the Pt coated template to the substrate to ensure good mechanical and electrical contact between the templated Pt film and the substrate. The resulting template-strip sample 'sandwiches' were placed in an oven for 10 min at 180 °C in order to cure the epoxy and then loaded into the UHV chamber for stripping and analysis.

The in-situ UHV template stripping process has been described in detail in a previous work [1]. In brief, a metal clasp is fashioned around the template that can be grabbed by a wobble stick to pull the template from the substrate in UHV. For this study, the bonded template-strip sandwiches were exposed to various annealing conditions (in UHV) prior to stripping the metal surfaces from the templates. To achieve this, the pre-stripped sandwiches were heated to a temperature of 140–150 °C for a period of either 0 h (no anneal), 18 h or 6 d.

As a benchmark against which to compare the TS surfaces, a single-crystal (SC) Pt(111) surface was also prepared and examined by UHV STM. The surface was generated by repeated exposures to a cycle that consisted of an initial argon ion-beam sputter clean, followed by an 800 °C anneal in an oxygen ambient of 10^{-8} Torr, which was then followed by an 800 °C anneal in UHV. The cycle was repeated until STM imaging verified an atomically clean surface.

The UHV annealing and stripping of the TS surfaces, as well as the Pt(111) single crystal preparation and STM examination of the surfaces were all carried out in an Omicron UHV VT STM/AFM system with a base pressure of 10^{-10} Torr.

3 Results

3.1 *Un-annealed surfaces*

Figure 1 shows two UHV STM images of a TS Pt surface that underwent no pre-strip anneal after the metal film deposition (other than the 10 min epoxy cure at 180 °C). This

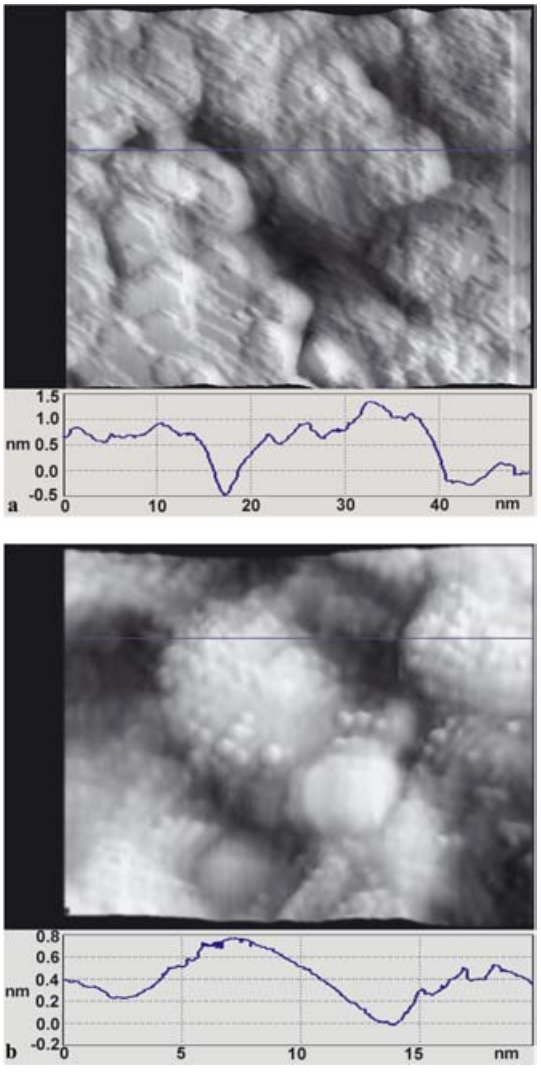

FIGURE 1 STM micrographs of un-annealed TS Pt surface grown at slow initial deposition rate of 0.1 Angstrom/s. (**a**) Region with well-defined crystallites in lower left quadrant imaged in constant current mode with 2.3 nA and 0.21 gap voltage (V_{gap}) (**b**) Region with ill-defined granular clusters imaged at constant current with -0.1 V_{gap} and 1.1 nA

surface was prepared using the slow metal deposition process that involved an initial deposition rate of 0.01 nm/s before a subsequent ramp up. As seen in Fig. 1a, the surface consists of a random assemblage of structures appearing to be of two types: those loosely composed of the granular clusters seen in the upper right quadrant of the image, and those that appear as smooth platelets without granular features that predominate in the lower left quadrant.

The smooth structures in this example are further distinguished by hexagons or truncated hexagons that define large regions of the platelets. In the example shown in the lower left of 1a, the platelets are stacked in a superstructure about 20 nm wide, which is bounded on its right side by a grain boundary and at its top by another, smaller set of platelets 10 nm wide. The planar surfaces of the smaller set are tilted ten degrees with respect to the planar surfaces of the superstructure. Although it was not possible to obtain atomically resolved images of these structures, it was possible to measure the step heights between overlapping platelets, and in this example that distance was 0.25 nm $\pm$ 0.01 nm averaged over five measurements.

Figure 1b shows examples of the smaller, granular structures composed of discrete granules with diameters ranging from 0.6–0.8 nm. While these structures are rich with features that demonstrate three- and six-fold symmetries, they are difficult to interpret, since the distances between features formed by the granules are not consistent with the spacing of atoms or planes in crystalline Pt. The individual granules are too large to be to be Pt atoms in a crystalline array and it can not be determined whether they are adatoms or clusters of atoms.

Figure 2 shows another surface that also underwent no pre-strip anneal, but was instead prepared using the fast metal deposition process that started and remained at 0.1 nm/s throughout the entire Pt film deposition. Whereas the surface initially grown at 0.01 nm/s displays a considerable number of the smooth platelets, the surface grown at a rate of 0.1 nm/s appears to be composed entirely of loosely agglomerated grains and clusters. Once again the granules range in size from 0.6–0.8 nm and are loosely organized into superassemblages. However, the platelets from the fast deposition process (Fig. 2) are more numerous, have a smaller average size distribution, and appear to be overlapping or stacked to a greater extent than those from the slow deposition process as seen in Fig. 1.

While the STM images do not identify the chemical species of the granular clusters, the observed prominent decrease in surface granularity with the slower Pt deposition process suggests the grains are composed of clusters of individual Pt and are not surface contaminants. The fact that both the granularity of the surface increases and the average platelet size decreases with the higher initial Pt deposition indicates that the initial mobility of the first layer(s) of Pt atoms deposited on the templating surface has a large influence on the final un-annealed TS Pt surface structure.

During the slow deposition process the first layers of Pt atoms arriving at the surface have a longer period in which to

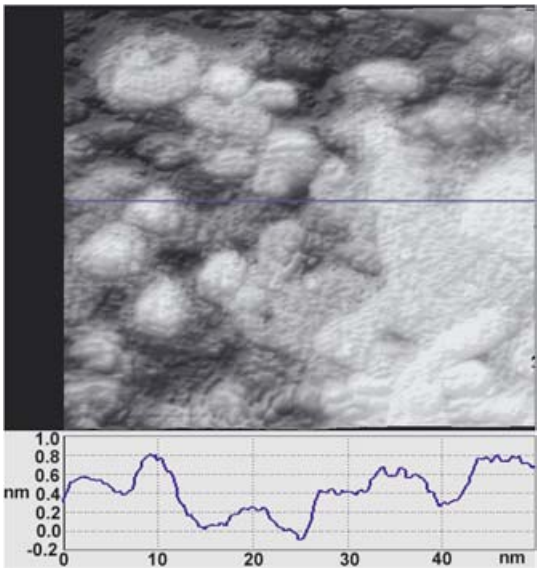

FIGURE 2 Constant-current STM micrograph of un-annealed TS Pt surface grown at fast deposition rate of 1 Å/s, (V_{gap} : -0.5 V, I : 1.0 nA)

diffuse and agglomerate into the larger discrete and smooth platelet structures. Conversely, during the high deposition rate, the Pt atoms have little time to diffuse before other Pt atoms arrive on the surface and limit the mobility at the template/Pt interface. As a result, the Pt atoms at the interface can become kinetically trapped in the observed small granular clusters.

A reasonable assumption is that the smooth platelets are, in fact, small nucleating crystallites that have developed crystallographic (111) planes oriented along the interface. This interpretation is supported by the sixfold symmetry of these features as well as by the measured height of $0.25\,\text{nm} \pm 0.01\,\text{nm}$ between neighbouring platelets or terraces associated with the platelets. Though this value is somewhat high compared to the accepted value of 0.226 nm for the interplanar spacing of Pt(111) planes, it does fall within the margin of error found for similar measurements on the benchmark single crystal Pt surface ($0.27\,\text{nm} \pm 0.08\,\text{nm}$).

Based on this understanding, the presumption would be that post-deposition annealing of the samples should provide additional opportunity for the rearrangement of kinetically trapped Pt atoms at the template/Pt interface, resulting in the decrease of the observed granularity, further increase in observed platelet size and the further development of oriented crystallographic surfaces.

3.2 *18 hour pre-strip vacuum anneal*

Shown in Fig. 3a is a $(100\,\text{nm})^2$ STM image of a template-stripped Pt surface produced by the slow deposition process and exposed to an 18 h pre-strip anneal at 150 °C in UHV. This image clearly demonstrates the expected absence of surface granularity and the growth in the average feature size. The randomly oriented platelets that dominated the un-annealed surface have been replaced by clean step edges and terraces of crystalline grains, supporting the hypothesis that the smoother platelets of the slow deposition process in the previous subsection were small nucleating crystallites. Estimates of the average grain size based on correlated step alignments are in the range of ~ 30–$40\,\text{nm}^2$, though individual grains ranging from ~ 15 nm to an upper limit around $\sim 100\,\text{nm}^2$ were observed.

Examination of Fig. 3a shows a surface consisting of a number of mesas or two dimensional islands a few nanometers in diameter stacked on top of one another, which in turn sit atop highly pitted planes and terraces ten to twenty nanometers in width with meandering edges. The average step height between neighbouring terraces was measured as $0.25\,\text{nm} \pm 0.02\,\text{nm}$ by averaging over ten separate measurements. This agreed well with the measured value of the benchmark single crystal (SC) Pt(111) as well as with the accepted value of 0.226 nm for bulk Pt(111) planes.

Atomically resolved images of the underlying terraces were also obtained and an example is shown in Fig. 3b, clearly demonstrating the hexagonal symmetry of a close-packed array of atoms. The nearest-neighbour distances were determined to be $0.27\,\text{nm} \pm 0.03\,\text{nm}$ using the location of the first order ⟨110⟩ reflections of fast Fourier transforms of the images. A similar analysis of the SC Pt surface yielded a value of $0.25\,\text{nm} \pm 0.03\,\text{nm}$. These values are both in good agreement

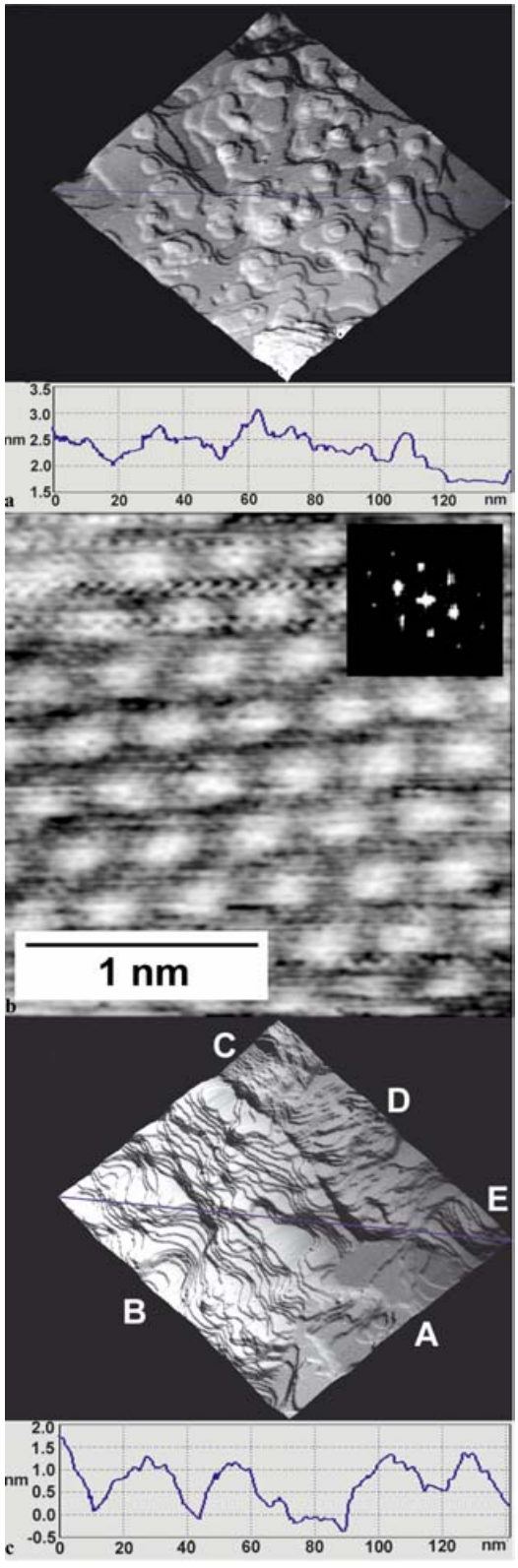

FIGURE 3 Constant – current STM micrographs of TS Pt surface grown at slow initial deposition rate of 0.1 Å/s and annealed for 18 h in UHV before stripping. (**a**) Region of surface with crystallite planes oriented parallel to the mean orientation of the templating surface, imaged at V_{gap} of 1.0 V and 1.0 nA. (**b**) High resolution STM image of a terrace surface. The *inset* depicts an FFT pattern of the surface showing the six-fold symmetry clearly evident in the image. Imaged at 0.45 V_{gap} and 133 nA. (**c**) Region of the surface where the planar orientation of the crystallites are misaligned with respect to each other. Image taken at -1.0 V_{gap} and 1.0 nA

with each other and with the expected value of 0.28 nm for the nearest neighbour distance of fcc Pt atoms in the (111) plane.

While the crystallites demonstrated in Fig. 3 are clearly oriented in the ⟨111⟩ direction, there are still striking differences between the TS and SC Pt surfaces. Shown in Fig. 4 is an image of the SC Pt surface at the same (100 nm^2) scan size of Fig. 3a. The two major differences between the SC Pt surface and TS Pt surface are the orientation of the step edges and the frequency of step bunching. Whereas the terrace edges in single crystal are straight and aligned along ⟨110⟩ orientations, the terrace edges of the TS Pt are highly facetted and meander across the surface of each crystallite. Moreover, in Fig. 4 significant bunching of the steps on the SC surface is clearly observable, while there is a roughly homogenous distribution of un-bunched steps across the TS surface in Fig. 3a.

These differences of the TS surface from the SC case are likely due to the interaction of the Pt atoms with the templating silicon-oxide surface. During annealing, the SC surface is exposed only to free-space UHV conditions, allowing for high mobility of atoms and step-edges along the surface. Thus, step edges form linearly along the lowest energy ⟨110⟩ directions and step edge pinning occurs only at infrequent defect sites, resulting in numerous steps clustering or bunching together at these defect sites. Conversely, the atoms and step edges at the TS Pt/template interface are highly constrained by the silicon-oxide template. For step bunching to occur on the TS surface, there would either have to be equivalent features on the underlying template (uncommon on ⟨100⟩ prime polished Si wafers) or else energetically unfavourable voids would have to form at the bunched Pt step edges.

Rather, the pinning locations and precise curvature of the step edges on the TS surface is likely related to a combination of the atomic features/defects on the silicon-oxide templates, as well as the nucleation, growth and coalescence conditions of the local Pt grains. The observed features on the TS Pt surface in Fig. 3(a) are reminiscent of the surface features formed by layers of native silicon-oxide on ⟨100⟩ silicon wafers similar to those used as the templates in this study [17]. Confirming this hypothesis will require a detailed exploration (planned for the near future) of the silicon-oxide surfaces used as the templates, in order to look for similar surface structures and features that may be mirrored by the TS surface. If nanoscale features of the silicon-oxide template can be reproducibly transferred to the TS metal surface, this opens the door for new method of transferring nanoscale features and patterns directly onto metal surfaces.

Although Fig. 3a represents a large portion of the surface sampled by STM measurements, a considerable portion of the surface also displayed regions of misaligned crystallites which are represented in Fig. 3c. More will be said about these regions in the next section.

3.3 *6 day pre-strip vacuum anneal*

Shown in Fig. 5 is a (120 nm)^2 STM image of a template stripped Pt surface produced by the slow deposition process and exposed to a 6 d pre-strip anneal at 150 °C in UHV. Figure 5 shows that the surface has become ordered into large-area, single crystal domains with crystallite widths of ∼ 100 nm, much larger than the ∼ 30–40 nm grain size of the 18 h annealed TS surface. In this particular example, four domains were observed, which are denoted by the letters A–D.

The crystalline grain designated "A" in Fig. 5 demonstrates an extremely similar qualitative appearance to the image of the 18 h annealed sample in Fig. 3a. While the terraces appear more uniform and smooth, and the average feature size has increased marginally, the degree of step curvature and meandering have remained nearly identical to the 18 h anneal sample. Despite the much longer annealing time of the 6 d sample, the level of step bunching and step alignment in this region of Fig. 5 is not markedly different from the 18 h anneal.

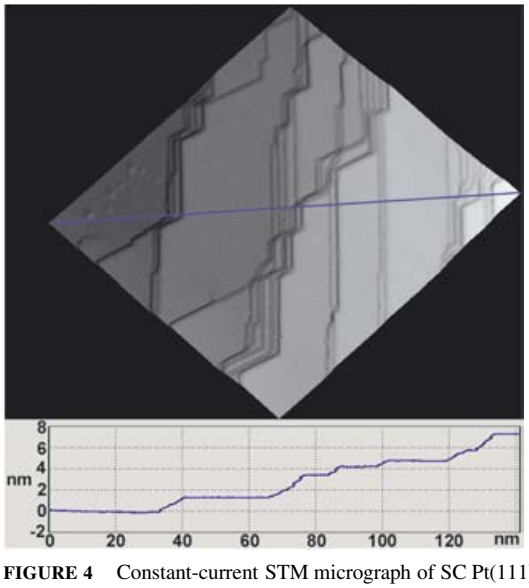

FIGURE 4 Constant-current STM micrograph of SC Pt(111) surface taken at −0.32 V_{gap} and 2.42 nA

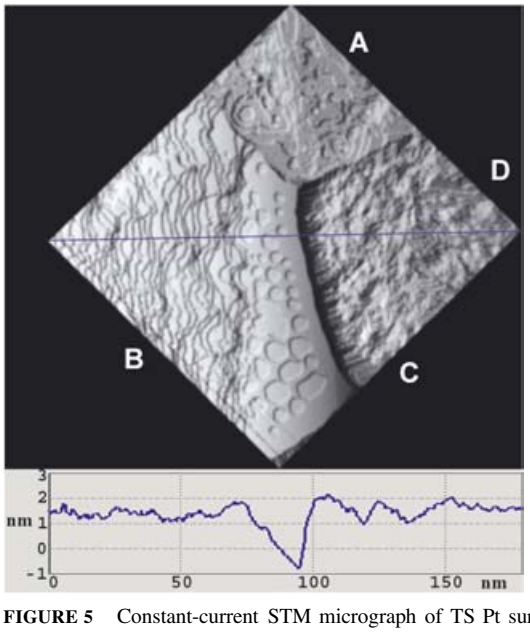

FIGURE 5 Constant-current STM micrograph of TS Pt surface grown at slow initial deposition rate and annealed for 6 d in UHV prior to stripping. Imaged at −0.76 V_{gap} and 1.1 nA

For this region of the image (and other images of numerous similar regions on the sample) the measured step heights were in agreement with (111) oriented steps, similar to those observed for the 18 h anneal. Atomically resolved images of these regions also revealed six-fold symmetry, however the nearest neighbour distances were twice those measured for the benchmark Pt crystal. This is indicative of a surface contaminant arranged in a 2×2 superlattice. Subsequent ex-situ X-ray photoelectron spectroscopy (XPS) confirmed the presence of silver adsorbates on the TS surface, indicating that the silver epoxy had diffused onto the surface. Between crystallites "B" and "C", a large fissure is clearly observable on the surface, and many such fissures and pits up to 50 nm wide are observable on large scan sizes. Since the crystal grains are on the order of the film thickness (assuming roughly isotropic grain size), single grain boundaries likely span the whole thickness of the Pt film and provide an easy diffusion pathway for components of the silver epoxy to reach the TS surface prior to stripping. XPS revealed no traces of silver on the 18 h anneal sample, indicating that the diffusion of the epoxy component to the surface is limited to the percolated grain pathways of the 6 d annealed sample.

Turning now to crystal domain "B", we note that the surface morphology is markedly different from both domain "A" and Fig. 3a. Rather than the crystallographic planes being aligned perfectly parallel with the planes of domain "A", the intersection of the two sets of planes describes an angle of 170 °C.

This is unexpected for the growth of the Pt crystallites in contact with a non-adhering, ultra-flat surface like the silicon-oxide template, as it would require energetically unfavourable void formations at the template/Pt interface. Rather, the lowest energy surface (in the case of Pt, the (111) surface) is expected to grow perfectly aligned and in intimate contact with the ultra-flat silicon-oxide template, as is indicated by Fig. 3a and crystallite "A". Instances of misaligned crystallites were observed for all three annealing conditions, however.

One possible explanation for this may lie in the local morphology of the template relative to a nucleating crystallite. Though crystallites can nucleate in any orientation, the ones most likely to survive a ripening process will be those with orientations that produce the lowest energy surfaces. At length scales on the order of a few nanometers, small variations in template roughness could lead to the formation of crystallites slightly out of alignment with neighbouring crystallites, but still in intimate contact with the template surface. Tables 1 and 2 summarize the angles made between planes of neighbouring crystallites observed in the 18 h and 6 d anneal. The angles were calculated by first taking vector cross products to determine unit normal vectors for each set of planes associated with a crystallite and then taking vector dot products of the normal vectors to calculate planar misorientations. With the exception of one highly misaligned crystallite labelled "C" in both examples, the surfaces are never misaligned more than 12 °C with respect to each other. It is not unreasonable to suppose that two crystallites, each nucleating on local regions of the template inclined from 3–6° to an imaginary plane defined by the mean height variation of the template, could grow to intersect each other at a cumulative misorientation of 10°.

	B	C	D	E
A	170°	167°	176°	171°
B	**X**	158°	170°	178°
C	**X**	**X**	163°	158°
D	**X**	**X**	**X**	172°

TABLE 1 Angles defined by the intersections of the terrace planes associated with crystallites "A" through "E" as denoted in Fig. 3c

	B	C	D
A	170°	165°	170°
B	**X**	159°	168°
C	**X**	**X**	163°

TABLE 2 Angles defined by the intersections of the terrace planes associated with crystallites "A" through "D" as denoted in Fig. 5

Interactions at the template film interface may not be the only factors governing the evolution of the surface, though. Subsequent ex-situ examination of TS surfaces produced using the Epo-Tek H 21D silver epoxy by optical microscopy showed the surfaces to have small corrugations and not the smooth mirror-like finish of TS surfaces produced with other epoxies [10]. These corrugations appeared on optically visible length scales of $\geq\sim 10\,\mu$m, significantly larger that the length scales easily accessible to rigorous STM examination. Exploration of the epoxy properties revealed that the fast cure method (10 min at 180 °C) used to prepare the TS samples actually causes significant non-uniform shifting of the epoxy film, resulting in substantial build up of mechanical stress on the 120 nm Pt films. This stress is likely to cause premature stripping and even cracking of the Pt film in several regions, resulting in the observed irregularities on optically observable length-scales. The prematurely-stripped regions would thus no longer remain in intimate contact with the underlying templating surface. When the annealing is carried out in UHV, these prematurely-stripped regions will obviously exhibit distinctly different crystallite growth behaviour than the regions of the Pt film still templated by the ultra-flat silicon-oxide surface. Most notably, the orientation of crystallites in these prematurely-stripped regions would not be constrained in the same way by intimate contact with the surface. This may be another explanation for the origin of the observed misaligned crystallites seen in the 18 h and 6 d annealed samples. In addition, the large fissures observed on the 6 d annealed sample could be the result of the mechanical stress in the epoxy pulling the grains apart, as well as the diffusion of the epoxy components between the crystallites (as evidenced by XPS) introducing further mechanical strain into the Pt film.

At this point, the collected data are insufficient to conclusively attribute the misaligned crystallites to one particular cause. What the 6 d anneal experiment has clearly revealed is the importance of the substrate-TS film bonding process. Artefacts strongly correlated with both the mechanical strain of the epoxy curing process and mobile components in the epoxy composition are visible in several of the samples examined in this study. The application of our previously demonstrated cold-weld based template-stripping [18] process to the UHV-STM TS samples is presently being developed in order to eliminate any epoxy related artefacts.

4 Discussion & conclusions

The data presented above revealed that the TS Pt surface morphology begins in an ill-defined clustered state with highly ordered features at small length scales immediately after Pt film deposition. While the deposition parameters were shown to affect the observed structure, the influence was minor compared to that of subsequent post-deposition annealing of the template/Pt system prior to being stripped. During post-deposition annealing, the TS surface morphology evolved rapidly from one defined by a poorly organized assemblage of nanocrystallites and clusters to one composed primarily of large-grained crystallites.

Figure 6a–c further demonstrates this TS surface evolution with three $(1\ \mu m)^2$ UHV-STM images of the different annealing conditions explored above (no anneal, 18 h and 6 d). Included with the STM images in Fig. 6 are statistical histograms showing the frequency values of the relative heights in each image. Table 3 summarizes the median height and RMS roughness values of the images in Fig. 6.

The distribution of heights on the TS surface, quantitatively measured by the full width half maximum (FWHM) of the histograms in Fig. 6, clearly decreases from the unannealed sample to the 18 h anneal. This is in good agreement with both the emergence of smooth oriented crystallite surfaces as observed in Fig. 3a and the decrease in roughness values listed in Table 3. However, this smoothening of the surface does not extrapolate from the 18 h anneal to the six day anneal. Rather, the FWHM of the histograms in Fig. 6 and the RMS roughness values in Table 3 reveal that a roughening of the surface beings to occur as the anneal progresses.

The increase in roughness that occurs between 18 h and 6 d can be attributed to rifting and pitting along grain boundaries. Though the data demonstrated that the crystallite grain size clearly continues to expand from the 18 h to 6 d anneal, and that the surface of each grain becomes (on average) progressively smoother with subsequent annealing [19], the cracks and fissures appearing between grains that are clearly observable in both Figs. 5 and 6c become the dominant contributors to surface roughness at the 1 μm size scale.

As discussed above, it cannot be determined from the present data whether this rifting is caused solely by the stresses that develop during the employed epoxy curing procedure or whether there are intrinsic mechanisms in the TS surface and film evolution process that drive this long-time annealing behaviour. The need for further experiments utilizing different epoxies or novel substrate bonding techniques such as cold-welding [18] is evident from these results to elucidate the mechanisms driving the TS surface roughening at longer time anneals, as well as to confirm the origin of the misaligned crystallites as an epoxy artefact.

Sample	Median Height Value	RMS Roughness Value
No Anneal	0.71 nm	0.46 nm
18 Hour Anneal	0.37 nm	0.26 nm
6 Day Anneal	0.55 nm	0.36 nm

TABLE 3 Median values and root-mean-square roughness values of heights measured over (1 micron)2 area of TS Pt surfaces annealed for (a) 0 time (b) 18 h, and (c) 6 d

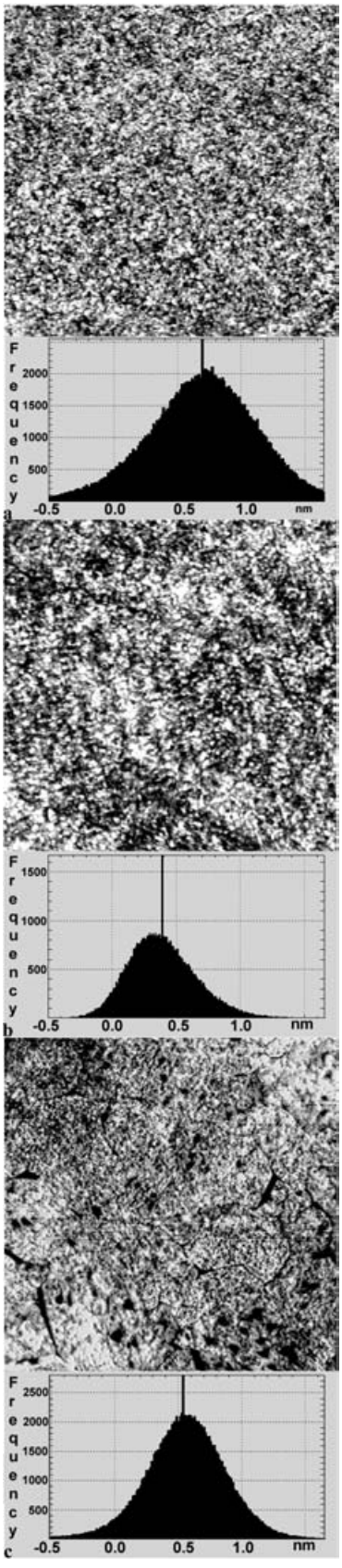

FIGURE 6 Height histograms along with corresponding STM micrographs of (1micron)2 region of TS Pt surfaces, all grown at slow initial deposition rates, bonded, and annealed in UHV for (**a**) 0 time, (**b**) 18 h, and (**c**) 6 d. Constant current imaging conditions for the three images were (**a**) $-0.23\ V_{gap}$, 2.0 nA, (**b**) $1.0\ V_{gap}$, 0.96 nA and (**c**) $-0.87\ V_{gap}$, 1.0 nA

What has been clearly resolved from the data in this study is the importance of post-deposition annealing of the template/Pt sample prior to the stripping step. For applications of TS surfaces such as SAM formation and molecular electronics, the granular structure of the un-annealed TS surfaces is highly undesirable. On the other hand, the 18 h post-deposition annealing process is shown to be nearly ideal for producing the smooth and oriented polycrystalline surfaces desirable for such applications. Though issues such as the misaligned crystallites, large-scale film corrugations and the development of fissures at grain boundaries with longer annealing times all require further study, the need for post-deposition, pre-strip annealing is still clearly illustrated and the 18 h anneal time is shown to be provide a very reasonable starting surface for iterative optimization to begin.

The basic model describing these results – whereby the mobility of Pt atoms at the template-surface drives the evolution of the final TS surface structure – also suggests that heating the templating substrates during the deposition of the Pt film could prove the optimum method of producing smooth crystallographic planes at the interface while providing a constant Pt flux which should prevent the formation of roughening fissures or voids at grain boundaries. Investigations of this additional TS surface fabrication parameter are presently being pursed.

The in-vacuo template-stripping process introduced previously [1] and employed herein offers a way of producing a variety of Pt surfaces that can be individually tailored for the exploration of a number of physical processes. Further studies of the un-annealed surfaces could provide valuable insight into thin film nucleation and growth mechanisms as it offers a unique way of accessing film-substrate interfaces. Alternatively, the smooth annealed surfaces could prove interesting for the study of catalytic processes and are already the focus of ongoing research in our lab into the deposition of densely packed SAMs for molecular electronics applications [20]. Although our studies have focused thus far on Pt exclusively, the process demonstrated should be equally applicable to all systems in which chemisorption between the film and substrate can be prohibited. It has already been demonstrated with previous work on other noble metals such as gold [10], but should work equally well for all metals that slowly oxidize or require elevated temperatures to produce silicides.

ACKNOWLEDGEMENTS The authors thank DARPA for partial funding of the research carried out at HP Labs, and JB thanks NSERC and iCORE for partial funding. The authors gratefully acknowledge Dimitre Karpuzov at the Alberta Center for Surface Engineering and Science (ACSES) for assistance with XPS data collection. The authors are also grateful to the technical resources division at Epoxy Technologies for assistance with evaluating epoxy curing conditions.

REFERENCES

1 R. Ragan, D. Ohlberg, R.S. Williams, J.J. Blackstock, S. Kim: J. Phys. Chem. B (2004), submitted
2 J.R. Heath, P.J. Kuekes, G.S. Snider, R.S. Williams: Science **280**, 1716 (1998)
3 P.J. Kuekes, R.S. Williams, J.R. Heath: US Patent (6,128,214, United States 2000)
4 A. Dehon: IEEE Trans. Nanotechnol. **2**, 23 (2003)
5 G. Snider, P.J. Kuekes, R.S. Williams: Nanotechnology **15**, 1 (2004)
6 Y. Chen, G.-Y. Jung, D.A.A. Ohlberg, X. Li, D.R. Stewart, J.O. Jeppesen, K.A. Nielsen, J.F. Stoddart, R.S. Williams: Nanotechnology **14**, 462 (2003)
7 J.J. Blackstock: In *Department of Physics* (University of Alberta, Edmonton, Canada, in preparation 2004)
8 M.S. Islam, Z. Li, D.A.A. Ohlberg, D.R. Stewart, Y. Chen, S.Y. Wang, R.S. Williams: unpublished results
9 J.J. Hickman, P.E. Laibinis, D.I. Auerbach, C. Zou, T.J. Gardner, G.M. Whitesides, M.S. Wrighton: Langmuir **8**, 357 (1992)
10 J.J. Blackstock, Z. Li, M.R. Freeman, D.R. Stewart: Surf. Sci. **546**, 87 (2003)
11 D. Stamou, D. Gourdon, M. Liley, N.A. Burnham, A. Kulik, H. Vogel, C. Duschl: Langmuir **13**, 2425 (1997)
12 R.H. Terrill, T.A. Tanzer, P.W. Bohn: Langmuir **14**, 845 (1998)
13 S.-S. Wong, M.D. Porter: J. Electroanalytical Chem. **485**, 135 (2000)
14 D. Losic, J.G. Shapter, J.J. Gooding: Langmuir **17**, 3307 (2001)
15 M. Kawasaki, H. Nagayama: Surf. Sci. **549**, 237 (2004)
16 The larger error on the single crystal surface is a result of the single crystal surface exhibiting prominent step bunching, making the measurement of a single atomic layer step more difficult
17 M. Horn-von Hoegen: (private communication, 2004)
18 J.J. Blackstock, Z. Li, G.-Y. Jung: J. Vac. Sci. Technol. B **22**, 602 (2004)
19 UHV-STM scans of (100 nm) by (100 nm) or less revealed that the surfaces of individual crystallites on the 6 d anneal sample were smoother than equivalent images of the 18 h annealed sample
20 J.J. Blackstock, Z. Li, D.R. Stewart, K. Isaacson, D.Y. Kwok, M.R. Freeman, J.-B.D. Green: J. Am. Chem. Soc. (2004), submitted